Computer Simulation of Electron Transfer Dynamics through a Fluctuating Protein

Qian Xie, Georgios Archontis and Spiros S. Skourtis

Department of Natural Sciences, University of Cyprus, Nicosia 1678, Cyprus

A central challenge of protein electron transfer theory is to understand how protein dynamics affects electronic tunneling from donor to acceptor. We studied this problem by use of computer simulation method. The central result is that electron transfer dynamics can be described by a time-dependent version of the two-state approximation, which amounts to the solution of a time-dependent Schrödinger equation drived by a time series of effective two-state Hamiltonians yielded by applying Löwdin's partitioning technique to the Hamiltonian of the whole system, obtained by using semiempirical all-valence-electron quantum chemical methods, for a series of conformations taken consecutively from an equilibrium molecular dynamics trajectory of the studied protein.

I. INTRODUCTION

In weakly coupled donor-acceptor systems, the rate of electron transfer(ET) reactions is given by the golden rule

$$k_{\mathrm{ET}} = \frac{2\pi}{\hbar}|T_{DA}|^2(\mathrm{F.C.}) \tag{1}$$

where T_{DA} is the effective electronic coupling matrix element between the donor and acceptor localized states and (F.C.) is the thermally weighted Frank-Condon overlap factor between donor and acceptor's nuclear vibronic manifolds. In an orthogonal basis, T_{DA} can be given by Larsson's equation

$$T_{DA}(E) = \sum_{b_i,b_j} H_{Db_i}\left[(E\mathbf{I}^b - \mathbf{H}^b)^{-1}\right]_{b_ib_j} H_{b_jA} \tag{2}$$

where b_i, b_j are localized bridge states that couple directly to donor and acceptor through the Hamiltonian matrix elements H_{Db_i} and H_{Ab_j}, $\mathbf{H}^b$ is the bridge Hamiltonian, $\mathbf{I}^b$ is a unity matrix which has the same dimension with the bridge Hamiltonian, and E is the tunneling energy. A theoretical issue for long-range ET in proteins is the reliable calculation of T_{DA}, and of more importance, how it is controlled by the structural motif of the mediate bridge (this is interesting because of its relevance to the engineering of ET)[1]. A tunneling pathway model has been developed by Beratan, Betts and Onuchic[2] to describe how the protein environment may influence T_{DA}. In their model, the intervening structure between donor and acceptor is decomposed into subunits linked by covalent bonds, hydrogen bonds, and through-space interactions(van der Waals contacts). Each link is associated with a decay factor, characterizing the decay of coupling strength with respect to length of the link. A graph-search algorithm is used to find the prevailing tunneling

pathways in proteins and to calculate their relative coupling strengths. A remarkable success of the tunneling pathway model was that it predicted that β-sheet structures would be more effective in ET than α helices, which has received strong support from experimental observations[3].

Since T_{DA} is structure-dependent, it may differ from one conformation to another. However, the value of T_{DA} for a given protein is usually calculated based on the standard conformation of the protein determined experimentally by X-ray cystallography. A question immediately arises here: Can the T_{DA} thus obtained be representative for the ET capability of the protein, which is actually moving around in physiological condition? The answer to this question does not seem very positive. Several groups have started to question about it[4,5]. It has been shown by Wolfgang et al. [4] that even modest structural fluctuations generated by standard molecular dynamics(MD) method can lead to changes of T_{DA} that are large enough to challenge conclusions drawn from electronic structure calculations on the basis of computations on individual geometries. We also found from our own calculations that T_{DA} may sometimes fluctuate around zero (presumably due to the effect of destructive interference). According to eq. (1), $T_{DA} = 0$ means that the electron can never transfer to the acceptor site.

A plausible idea to fix the problem is to introduce an average T_{DA}, for example, the root mean square $\sqrt{\langle T_{DA}^2 \rangle}$, over an ensemble of conformations, to the rate expression eq.(1)[5]. Computationally, this ensemble of conformations can be a large number of snapshots randomly taken from a MD trajectory. Strictly speaking, $\sqrt{\langle T_{DA}^2 \rangle}$ would statistically represent the ET rate well only if an ET reaction could take place in no time. Nevertheless, tunneling is a dynamic event. During a tunneling process, the Hamiltonian governing the electronic motion evolves simultaneously with the propogation of electronic wave function. Therefore the tunneling of electron depends upon a Hamiltonian time series rather than just a single Hamiltonian or an average one. It remains a question how an electron will respond to the fluctuations of protein environment. Could the actual electronic propogation through a vibrating protein structure in a given time t be described simply by the average electronic coupling over the same period $\sqrt{\langle T_{DA}^2 \rangle_t}$?

We shall present in this paper a systematical computer simulation study for the above problems. The strategy is to investigate the quantum dynamics of a tunneling electron in a fluctuating external field provided by a protein environment. The basic assumptions we made are as follows: (a) The protein dynamics is treated classi-

cally: This assumption implies that the nuclear motion is completely decoupled from electronic degrees of freedom, particularly, the nuclear motion is not affected by an electron tunneling event; (b) The electronic motion is treated quantum mechnically: It is assumed that the tunneling electron obeys the single-particle time-dependent Schrödinger equation $i\hbar\partial\Psi/\partial t = H(t)\Psi(t)$; (c) $H(t)$, the Hamiltonian for an excess electron in the interior of a protein at time t, is given by the single-particle Hamiltonian obtained for the protein conformation at time t(for instance, the converged Fock matrix yielded by self-consistent field computation): This assumption means that the tunneling electron obeys the ground-state picture and single-particle protocol in the same way as the valence electrons do, as a result it experiences the same Hamiltonian as the other electrons do; Furthermore it means that the valence electrons belonging to atoms around donor and acceptor and along the tunneling pathways do not feel the tunneling of the excess electron, in another word, the electronic structure of a protein is not distorted by tunneling. The readers have to bear in mind that the conclusions we are going to draw about protein ET dynamics in this paper are based on these three general assumptions.

Some of our major results have been presented in a letter[6]. In this paper, we shall give the details about our simulations. The paper is organized as follows. The time-dependent Schrödinger equation in a fluctuating nonorthogonal basis is given in Section II. In the same section, we also discuss the calculation method for the nonadiabatic coupling matrix elements. The two-state and general multi-state reductions using Löwdin's partitioning technique are presented in Section III and IV. Technical details about the computer simulation are discussed in Section V. To mention a few, the simulation of protein nuclear dynamics was carried out by using the molecular simulation package CHARMM[7], and the Natural Bond Orbitals(NBO) method[8] was used to transform the Schrödinger equation from atomic orbital (AO) basis into bond orbital (BO) basis. Results and discussions are presented in Section VI. Section VII concludes the paper.

II. TIME-DEPENDENT SCHRÖDINGER EQUATION IN A FLUCTUATING NONORTHOGONAL BASIS

In this Section, we derive the formulism of the time-dependent Schrödinger equation in a fluctuating nonorthogonal basis. We start from the operator form of the Schrödinger equation

$$i\hbar\partial_t|\Psi(t)\rangle = \hat{H}(t)|\Psi(t)\rangle \qquad (3)$$

where $\Psi(t)$ is the electronic wave function at time t, $\hat{H}(t)$ is the Hamiltonian at time t, and $\hbar$ is the Planck constant. Assume we have a time-dependent nonorthogonal

basis set $|\alpha(t)\rangle$, the overlap matrix is also time-dependent $S_{\alpha\beta}(t) = \langle\alpha(t)|\beta(t)\rangle$. The basis functions satisfy the normalization condition at any time

$$\hat{I} = \sum_{\alpha\beta}|\alpha(t)\rangle\left[S^{-1}\right]_{\alpha\beta}\langle\beta(t)| \qquad (4)$$

To study the propogation of an electron in such a basis is to compute $\langle\alpha(t)|\Psi(t)\rangle$. Inserting the identity operator into both sides of eq.(3) and projecting $\Psi(t)$ onto α yields

$$\sum_{\gamma\delta}i\hbar\langle\alpha|\partial_t\gamma\rangle\left(\left[S^{-1}\right]_{\gamma\delta}\langle\delta|\Psi\rangle\right)$$
$$+\sum_{\gamma\delta}i\hbar\langle\alpha|\gamma\rangle\partial_t\left(\left[S^{-1}\right]_{\gamma\delta}\langle\delta|\Psi\rangle\right)$$
$$=\sum_{\gamma\delta}H_{\alpha\gamma}\left(\left[S^{-1}\right]_{\gamma\delta}\langle\delta|\Psi\rangle\right) \qquad (5)$$

Two different notations for the wave function can be introduced

$$\langle i(t)|\Psi(t)\rangle = d_i(t)$$

$$\left[S^{-1}(t)\vec{d}(t)\right]_i = x_i(t)$$

where $\vec{d} = (d_1, d_2, \cdots, d_N)$, N is the electronic dimension of the system. Correspondingly the Schrödinger equation becomes

$$i\hbar\partial_t\vec{x}(t) = S^{-1}(t)\left[H(t) - i\hbar K(t)\right]\vec{x}(t) \qquad (6)$$
$$i\hbar\partial_t\vec{d}(t) = \left[H(t) + i\hbar L(t)\right]S^{-1}(t)\vec{d}(t) \qquad (7)$$

where $K_{\alpha\beta}(t) = \langle\alpha(t)|\partial_t\beta(t)\rangle$ and $L_{\alpha\beta}(t) = \langle\partial_t\alpha(t)|\beta(t)\rangle$. To derive eq.(7), we see from the first derivative of the equality $\sum_\gamma S_{\alpha\gamma}[S^{-1}]_{\gamma\delta} = \delta_{\alpha\delta}$ that

$$\sum_\gamma S_{\alpha\gamma}\partial_t\left[S^{-1}\right]_{\gamma\delta} + \sum_\gamma\langle\alpha|\partial_t\gamma\rangle\left[S^{-1}\right]_{\gamma\delta}$$

$$= -\sum_\gamma\langle\partial_t\alpha|\gamma\rangle\left[S^{-1}\right]_{\gamma\delta}$$

If the basis functions are orthonormal, $S(t) = I$, then $K(t) = -L(t)$ (because $\langle\partial_t\alpha|\beta\rangle + \langle\alpha|\partial_t\beta\rangle = 0$), we find eqs.(6) and (7) are identical.

The site occupancy is defined as the diagonal elements of the following matrix $P_i(t) = \rho_{ii}(t)$

$$\rho(t) = S^{-1}(t)\vec{d}(t)\vec{d}^\dagger(t) = S(t)\vec{x}(t)\vec{x}^\dagger(t) \qquad (8)$$

For computational convenience, we adopt the second notation $(\vec{x})$ in our calculations.

Eqs.(6) or (7) tells us that to understand the ET dynamics of an electron in an interested system we need to know three time series $S(t)$, $H(t)$ and $K(t)$ or $L(t)$ for

2

it. While obtaining $S(t)$ and $H(t)$ is straightforward, the calculation of $K(t)$ or $L(t)$ is more complicated. We shall discuss more about it in the following.

If we choose a localized basis for a time-dependent calculation, we have to address the problem of fluctuating basis since localized basis fluctuates as atomic configuration fluctuates. The K or L term is called the nonadiabatic coupling (NAC) matrices [9,10]. The NAC matrix elements can be rewritten as

$$K_{ij}(t) = \dot{\mathbf{R}}_j \cdot \langle \Phi_i(\mathbf{R}_i) | \frac{\partial}{\partial \mathbf{R}_j} \Phi_j(\mathbf{R}_j) \rangle \qquad (9)$$

if the wave function Φ_i depends only on the position $\mathbf{R}_i$ of the nucleus to which orbital i belongs. One can see from the above equation that for a stable protein whose atoms vibrate in the vicinities of their thermal equillibrium positions, the contributions from the nonadiabatic effect are of the magnitude of phonons, which is usually much smaller than the strength of electronic couplings. Another property of the NAC matrix elements is its temperature dependence. The effect of K_{ij} on ET dynamics (and the so-called electronic friction for MD[9]) diminishes when the system cools down. For a liquid whose atoms move wild and rapidly, the NACs may turn out to be very important.

A simple idea to calculate the NAC matrix elements is to introduce the concept of *advanced and retarded overlaps*. In fact the NAC matrix element can be approximated by a differential form

$$\langle \Phi_i \mid \partial_t \Phi_j \rangle \approx$$
$$\frac{1}{2\delta t} \left[\int \Phi_i^t(r) \Phi_j^{t+\delta t}(r) d^3 r - \int \Phi_i^t(r) \Phi_j^{t-\delta t}(r) d^3 r \right] \quad (10)$$

where δt is the time steplength, the first term in the right hand side is called the advanced overlap, the second the retarded overlap. These overlaps mean the overlaps of an orbital with another one at different time. Let us just forget about the time coordinate temporarily, assume the atom associated with the orbital index i is at the position where it is going to be at $t + \delta t$ or has been at $t - \delta t$, and calculate these advanced and retarded overlap integrals as if they were usual ones.
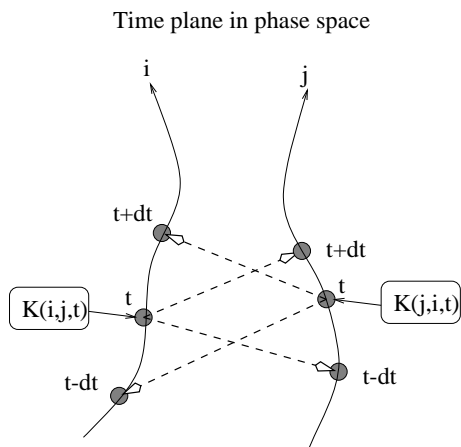
Time plane in phase space

In a generic nonorthonormal basis, K is not necessarily an antisymmetric matrix (therefore $H - i\hbar K$ is not a Hermitian), since in general $|\langle \Phi_j | \partial_t \Phi_i \rangle| \neq |\langle \Phi_i | \partial_t \Phi_j \rangle|$ (see Fig. 1). But if the basis is orthonormal, it has to be an antisymmetric one in order to guarantee that the operator in the right hand side of eq.(6) is a Hermitian, which is a necessary requirement from the conservation law of particle numbers in an orthonormal basis.

III. THE TIME-DEPENDENT TWO-STATE PICTURE

In a nonorthogonal basis, the effective two-state Hamiltonian matrix elements at time t are obtained by applying the Löwdin partitioning technique to the Hamiltonian matrix $\mathbf{H}(t)$ of the whole system, as follows

$$\mathcal{H}_{DD}^E(t) = H_{DD}(t) + T_{DD}^E(t) \qquad (11)$$

$$\mathcal{H}_{DA}^E(t) = H_{DA}(t) + T_{DA}^E(t) \qquad (12)$$

$$\mathcal{H}_{AA}^E(t) = H_{AA}(t) + T_{AA}^E(t) \qquad (13)$$

with

$$T_{DD}^E(t) = \sum_{b_i,b_j} (E S_{Db_i}(t) - H_{Db_i}(t))$$
$$\times \left[\left(E\mathbf{S}^{\mathrm{br}}(t) - \mathbf{H}^{\mathrm{br}}(t) \right)^{-1} \right]_{b_i b_j} \left(E S_{b_j D}(t) - H_{b_j D}(t) \right)$$
$$(14)$$

$$T_{DA}^E(t) = \sum_{b_i,b_j} (E S_{Db_i}(t) - H_{Db_i}(t))$$
$$\times \left[\left(E\mathbf{S}^{\mathrm{br}}(t) - \mathbf{H}^{\mathrm{br}}(t) \right)^{-1} \right]_{b_i b_j} \left(E S_{b_j A}(t) - H_{b_j A}(t) \right)$$
$$(15)$$

$$T_{AA}^E(t) = \sum_{b_i,b_j} (E S_{Ab_i}(t) - H_{Ab_i}(t))$$
$$\times \left[\left(E\mathbf{S}^{\mathrm{br}}(t) - \mathbf{H}^{\mathrm{br}}(t) \right)^{-1} \right]_{b_i b_j} \left(E S_{b_j A}(t) - H_{b_j A}(t) \right)$$
$$(16)$$

3

where E is the tunneling energy, which is normally close to $H_{DD}(t), H_{AA}(t)$ (for convenience, we shall drop off the superscript E, and denote H_{DD} by E_D and H_{AA} by E_A), D, A, b_i stand for the donor, acceptor and the bridge states respectively, and $\mathbf{S}(t)$ is the overlap matrix at time t. $H_{DA}(t)$ represents the through-space interaction, which is usually very small in long-range ET (and sometimes we neglect it). $T_{DA}(t)$ is the conventional superexchange coupling in literature, while $T_{DD}(t)$ and $T_{AA}(t)$ are the backscattering matrix elements which are introduced to account for the interactions of donor and acceptor with their local environment. As is well-known, T_{DA} decays exponentially with respect to the increasing of the separation distance between donor and acceptor, whereas T_{DD} and T_{AA}, which represent in nature the local electronic properties around the donor and acceptor, have nothing to do with the length of the bridge (Fig. 2). A common property of the three matrix elements is that they share the same poles in the energy domain, namely, when the tunneling energy approaches the bridge eigenstates, they diverge and consequently the two-state approximation (2SA) breaks.
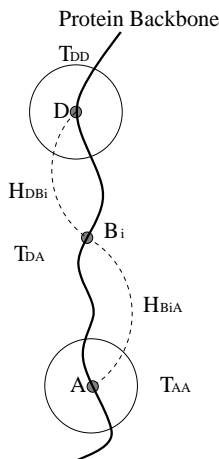
FIG. 2. A complete two-state picture for protein electron transfer. The backscattering matrix elements T_{DD} and T_{AA} rest upon the local environment around donor and acceptor, represented by the two circles in the figure.

In contrast to the well-known importance of T_{DA}, the role of T_{DD} and T_{AA} has not been explicitly mentioned, to our knowledge. This may be due to the fact that most of previous T_{DA} calculations were devoted to finding the resonant electronic states. The energies of donor and acceptor states have to be varied such that the system reaches resonance. In the case of resonance, $\mathcal{H}_{DD} \approx \mathcal{H}_{AA}$, which means that the effective two state system is on resonance as well. In fact, the role of the backscattering matrix elements in the static case is apparent: If we rewrite the resonance condition for the two state system: $E_D + T_{DD} \approx E_A + T_{AA}$, we shall see the energy shift required for resonance is $E_D - E_A \approx T_{AA} - T_{DD}$. The reason that $E_D = E_A$ is always not the resonance condition for a real protein is owing exactly to the fact that the local chemical structures surrounding donor and acceptor are always distinct.

In the absence of the Landau-Zener fluctuation, namely, when the donor and acceptor are energetically static, T_{DD} and T_{AA} will become important. In such a case, $T_{DD} - T_{AA}$ acts as an effective driving force which brings the donor and acceptor in and off resonance with frequencies resting on the motion of the local environment around the donor and acceptor rather than the donor and acceptor themselves. On the other hand, even in the presence of the fluctuations of potential energy surfaces E_D and E_A, T_{DD} and T_{AA} may either prolong or shorten the time in which the system remains in resonance, or, when $T_{DD} - T_{AA}$ is comparable in magnitude with $E_D - E_A$, increase or decrease the times of Landau-Zener crossing. Due to the localization property of backscattering, the fluctuations of T_{DD} and T_{AA} are not completely uncorrelated with those of E_D and E_A. The total driving force $\mathcal{H}_{DD} - \mathcal{H}_{AA}$ is in fact the result of concerted motion of donor, acceptor and their surroundings (interrelated by the Newtonian equations of motion in the MD simulation). Hence T_{DD} and T_{AA} are not completely stochastic additions to the effective potential energy surfaces (though they can be regarded as some kind of heat bath or dynamic energy disorder).

In the above discussion, we describe the two state reduction which simplifies a complicated protein ET system greatly into a two state model, and the physical meaning of the reduced system. In the context of time-dependence, such a procedure would be justified only when the following Schrödinger equation reproduces approximately the electronic propogation between donor and acceptor in the entire ET system

$$i\hbar\frac{d}{dt}\left[\begin{array}{c}\Psi_D(t)\\\Psi_A(t)\end{array}\right] = \left[\begin{array}{cc}\mathcal{H}_{DD}^E(t) & \mathcal{H}_{DA}^E(t)\\\mathcal{H}_{DA}^E(t) & \mathcal{H}_{AA}^E(t)\end{array}\right]\left[\begin{array}{c}\Psi_D(t)\\\Psi_A(t)\end{array}\right] \quad (17)$$

The overlap matrix element $S_{DA} = S_{AD}$ has been omitted since in long-range ET it is negligible, $S_{DD} = S_{AA} = 1$ if we assume that the states have been normalized, therefore, the overlap matrix is dropped off in the above equation. In the absence of a general analytical solution, eq. (17) can be solved if the Hamiltonian $\mathcal{H}$ is time-independent (Appendix A).

We shall prove in this paper that eq.(17) can reproduce the exact ET dynamics within a certain amount of time (normally a few hundred femtoseconds with a constant tunneling energy E). This statement, which we call the time-dependent two-state approximation (TD2SA), was repeatedly proven valid in a series of computations for azurin β-sheet with various donor-acceptor pairs (hence different levels of T_{DA}). The detailed numerical results will be presented in Section VI. The following discussion is based on the preconception that the TD2SA works.

Here we discuss the question raised in the Introduction: Can an average of $T_{DA}(t)$ be a good approximation in expressing ET rate? Considering a two-state system in which the donor and acceptor are kept in resonance

(not necessarily fixed) forever while T_{DA} is fluctuating, the transfer probability from donor to acceptor can be explicitly written as

$$P_{DA}(t) = \sin^2\left[\frac{1}{\hbar}\int_0^t T_{DA}(\tau)d\tau\right] \tag{18}$$

provided that the electron is at the donor site when $t = 0$. If we do not consider the fluctuation of $T_{DA}(t)$ but replace it with some sort of average, for instance, its root mean square $\sqrt{\langle T_{DA}^2\rangle_T}$ (where T is the time length for the average), we will obtain the following transfer probability $P_{DA}^{Ave\cdot}(t) = \sin^2\left[\frac{1}{\hbar}\sqrt{\langle T_{DA}^2\rangle}t\right]$. Obviously the actual dynamic behavior may be different from the sinusoidal one described by the latter. For example, if we assume that $T_{DA}(t)$ can be expanded into a cosine series $T_{DA}(t) = \frac{a_0}{2} + \sum_{n=1}^{\infty} a_n\cos(n\omega t)$ (where $\omega = 2\pi/T$), then $\sqrt{\langle T_{DA}^2\rangle} = \sqrt{\left(\frac{a_0}{2}\right)^2 + \frac{1}{2}\sum_{n=1}^{\infty}a_n^2}$, whereas the actual transfer probability is $P_{DA}(t) = \sin^2\left[\frac{1}{\hbar}\left(\frac{a_0}{2}t + \sum_{n=1}^{\infty}\frac{a_n}{n\omega}\sin(n\omega t)\right)\right]$. It is clear that the actual transfer probability is affected by not only the Fourier coefficients a_n but also the frequencies (but taking the average of T_{DA} washes out the the latter effect). The importance of frequencies is obvious for an extreme case when $T_{DA}(t)$ vibrates with a single high frequency mode $T_{DA}(t) = \hbar\omega\cos(n\omega t)$ (where $n \gg 1$). In this case, $\sqrt{\langle T_{DA}^2\rangle} = \hbar\omega/\sqrt{2}$, while $P_{DA}(t) \leq \sin^2(1/n)$, which means that the ET rate is actually very small.

Despite of its simplicity, the above analysis has shown a circumstance under which the average of T_{DA} cannot depict dynamic ET. In real proteins, particularly those systems with strong interference effect, we may encounter a similiar failure if we were to represent ET by an average T_{DA}.

Although it has been shown that T_{DD} and T_{AA} do play a role on ET reaction, it does not seem that the tunneling pathway model has to be modified to take them into consideration, due to their localization property. Yet, a more intriguing question is how to incorporate the dynamic effect into the pathway model. The concept of tunneling pathways is based on spatial decomposition of T_{DA}. If the potential energy profiles along different pathways become time-dependent, would the perturbations due to thermal fluctuations become large enough to reshuffle the relative importance of pathways, namely, to overthrow the dominance of the major pathways(if they exist)? If the answer is negative, one can surmise that ET reactions may really happen through pathways. Although in this paper we are not going to envisage the time dependence of tunneling pathways, it should merit more investigations in the future.

IV. GENERAL MULTI-STATE REDUCTION FOR ELECTRON TRANSFER

We have shown in the above section that the TD2SA presents a largely simplified picture for studying complicated ET dynamics in proteins. If, however, a bridge state joins resonance with the donor and acceptor, the two-state picture may fail. Such a case invites an extra reduced state to describe the motion of the third resonant state.
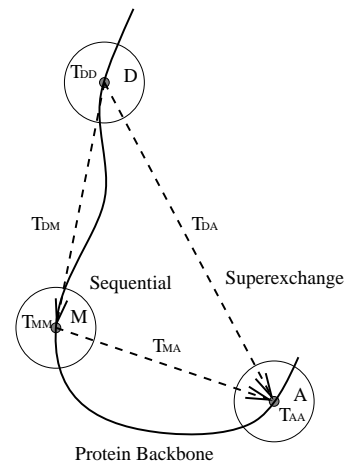
FIG. 3. Three-center electron transfer model. The redox center D is the origin(donor), M is the intermediate site (middle acceptor), and A is the destination(final acceptor).

We introduce here a general framework for the multi-state reduction (MSR). Let us assume that we would like to do a n state reduction for a protein electronic structure which consists of N orbitals. The n orbitals are labeled as $p_1, p_2, \cdots, p_n$, while the remaining orbitals (the bridge) as $b_1, b_2, \cdots, b_{N-n}(N \gg n)$, the reduced matrix elements are given by using the projection technique

$$\mathcal{H}_{p_ip_j}^E(t) = H_{p_ip_j}(t) + T_{p_ip_j}^E(t) \tag{19}$$

$$T_{p_ip_j}^E(t) = \sum_{b_i,b_j}[ES_{p_ib_i}(t) - H_{p_ib_i}(t)] \times$$

$$\left\{\left[E\mathbf{S}^{\text{br}}(t) - \mathbf{H}^{\text{br}}(t)\right]^{-1}\right\}_{b_ib_j}[ES_{b_jp_j}(t) - H_{b_jp_j}(t)] \tag{20}$$

Similiar to the two-state reduction scheme, the final goal of the MSR is to approximate the ET dynamics of the real system with a reduced time-dependent Schrödinger equation in which the reduced Hamiltonian is given in the above projected form: $i\hbar\partial_t\Psi = \mathcal{H}^E\Psi$.

Let us study an ET system which has three redox centers, denoted by D, M, and A, respectively(Fig. 3). There are two possible types of ET reactions in a three-center system[11]. The first one is the superexchange mechanism: $D^*\cdots A \longrightarrow D^+\cdots A^-$. The second one is the sequential mechanism: $D^*\cdots M\cdots A \longrightarrow D^+\cdots M^-\cdots A \longrightarrow$

$D^+ \cdots M \cdots A^-$. Three-center ET kinetics follows the superexchange pattern when the intermediate state M is off resonance with the donor and acceptor. In the resonance regime, the sequential pattern occurs where the intermediate site is also populated. For the same three-center system, the ET reaction should be much faster in the sequential channel than in the superexchange channel.
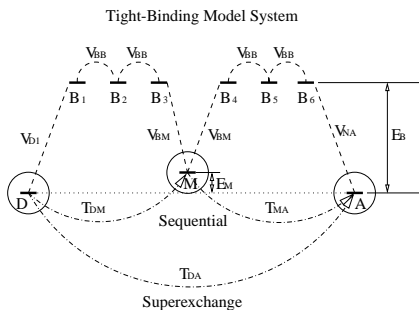
FIG. 4. A nine-state tight-binding model system. The site energies of all bridge states equal E_B, the energies of the donor and acceptor are zero, the intersite couplings are V_{BB} (bridge-bridge), V_{D1} (donor-bridge), V_{BM} (intermediate state-bridge), and V_{NA} (bridge-acceptor), non-nearest-neighbor interactions are neglected. The site energy of the intermediate site E_M is adjusted to drive the system into various transfer patterns.

In this Section, we shall discuss the three-center reduction with a simple tight-binding model (which is analogous to the Hückel model), since three-center ET reactions are relatively unfamiliar and we would like to establish a clear-cut picture before handling genuine systems. Studies for proteins will be given in Section VI.

Fig. 4 illustrates the tight-binding model for our study. For simplicity, we have chosen a homogenous system in which all the bridge sites have the same energy ($E_B = 4$, arbitrary unit) and all the intersite couplings are identical ($V_{D1} = V_{NA} = V_{BM} = V_{BB} = 1$), consequently the backscattering matrix elements for D and A are equal (this saves us efforts to tune them into resonance). Because of the difference of surroundings, the backscattering for the low-lying intermediate state differs from those for D and A. Therefore, the three-state resonance condition is not intuitively $E_D = E_M = E_A$. For a given static system, the transfer probilities from D to M and D to A oscillate with specific frequencies. The three-state resonance conditions can be found by computing the maximum electronic occupancy tunneled via the M site in several oscillation periods. Fig. 5 shows that $|E_M - E_D|$ for resonance increases when the couplings between M and its neighboring sites (V_{MB}) turn stronger. When $V_{MB} = 2$, this value is approximately 1.75, which is almost in the middle of the gap. This example demonstrates for a model three-state system the conspicuous dependence of the sequential resonance condition upon the electronic structure around the intermediate state.
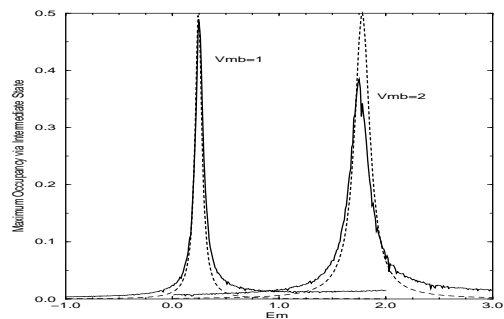
FIG. 5. Maximum occupancy transfered via the dynamically populated intermediate state as a function of its energy. Three-state resonance associated with sequential tunneling mechanism occurs around $E_M \approx 0.25$ when $V_{MB} = 1$ and $E_M \approx 1.75$ when $V_{MB} = 2$. Tunneling energy was chosen as -0.35 for the former case and -0.19 for the latter. Full lines represent the exact results; Dashed lines represent those of the 3SA(eq.(21)).

The 2SA cannot depict precisely the ET dynamics via an intervening state when the system enters the sequential transfer regime where a large part of occupancy goes through the middle state. A three-state approximation(3SA) has to be introduced

$$i\hbar \frac{d}{dt} \begin{bmatrix} \Psi_D(t) \\ \Psi_M(t) \\ \Psi_A(t) \end{bmatrix} = \begin{bmatrix} \mathcal{H}^E_{DD} & \mathcal{H}^E_{DM} & \mathcal{H}^E_{DA} \\ \mathcal{H}^E_{MD} & \mathcal{H}^E_{MM} & \mathcal{H}^E_{MA} \\ \mathcal{H}^E_{AD} & \mathcal{H}^E_{AM} & \mathcal{H}^E_{AA} \end{bmatrix} \begin{bmatrix} \Psi_D(t) \\ \Psi_M(t) \\ \Psi_A(t) \end{bmatrix}$$

(21)

where the effective three-state Hamiltonian matrix elements are obtained by using eqs.(19) and (20).

6

(a)
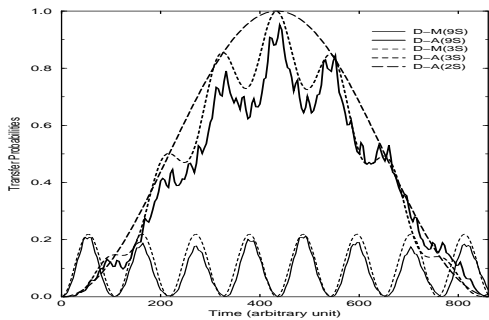
(b)
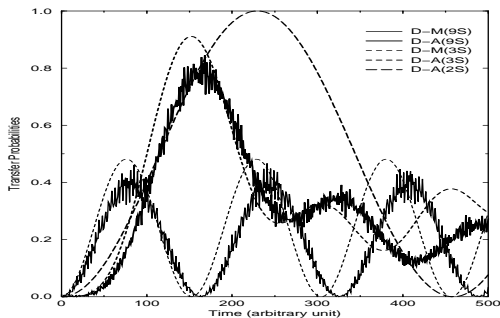
FIG. 6. Comparison of electronic propogation results produced by the exact, 2SA and 3SA methods for the tight-binding model system in the sequential transfer regime. (a)$E_M = 0.2$, $E_{tun}^{2s} = -0.34$, $E_{tun}^{3s} = -0.35$; (b)$E_M = 0.24$, $E_{tun}^{2s} = -0.285$, $E_{tun}^{3s} = -0.28$.

Fig. 6(a) shows that the 3SA can reproduce the exact dynamics perfectly when $E_M = 0.2$. One can see that in this case the 2SA can somewhat describe the transfer dynamics between D and A with a slightly different tunneling energy, since the transfer dynamics between D and A still resembles the sinusoidal behavior. But when E_M is increased to 0.24, resemblance to sinusoidal behavior vanishes, as is shown in Fig. 6(b). The time evolution cannot be attributed to a two-state mode. By comparison, the 3SA does much better, albeit its performance is not as impressive as shown in Fig. 6(a). In Fig. 5, we also show that the maximum population transfered through the middle site M versus E_M can be approximately reproduced by the three-state model. As expected, the 3SA deteriorates when the localization of M weakens (V_{BM} becomes greater).

The above analysis is not merely for improving the 2SA. As was pointed out by Ulstrup and coworkers[12], some of the most exciting chemical and biomolecular ET systems involve more than two reaction centers. Multistep ET and dynamically populated intermediate states ("hot" electronic states) in such systems has become central concepts in the new areas of ultrafast(femtosecond) processes. Our MSR approach provides, from rigorous electronic structure point of view, an effective multicen-

ter picture for such type of multi-channel ET reactions.

V. COMPUTATIONAL DETAILS

Fig. 7 shows the flowchart of our computer simulation. Before we proceed to the details, we would like to classify three time scales at first. The first time scale is the ET time steplength, which is the steplength used in integrating the Schrödinger equation, denoted by δt_{ET}; The second refers to the MD time steplength, which is the steplength chosen to integrate the classical equation of motion for protein, denoted by δt_{MD}; The third is called by us as the sampling steplength, which means the time interval between two neighboring sample Hamiltonians or sample conformations taken from a MD trajectory, denoted by δt_{SP}. The relation for these three steplengths is $\delta t_{ET} \ll \delta t_{MD} \leq \delta t_{SP}$.

An important issue about the time steplength is how short δt_{SP} should be in order not to skip over the contribution of the fastest motion of proteins to the ET dynamics. It is known that harmonic vibrations of bond lengths and angles generate the highest frequencies in proteins, and the time scale for this type of motion is at the level of femtoseconds[13]. Based on tests for a small diglycine, we found that the results of electronic dynamics with different δt_{SP} converged when it approached a femtosecond. Therefore, one femtosecond can be used as the sampling steplength.
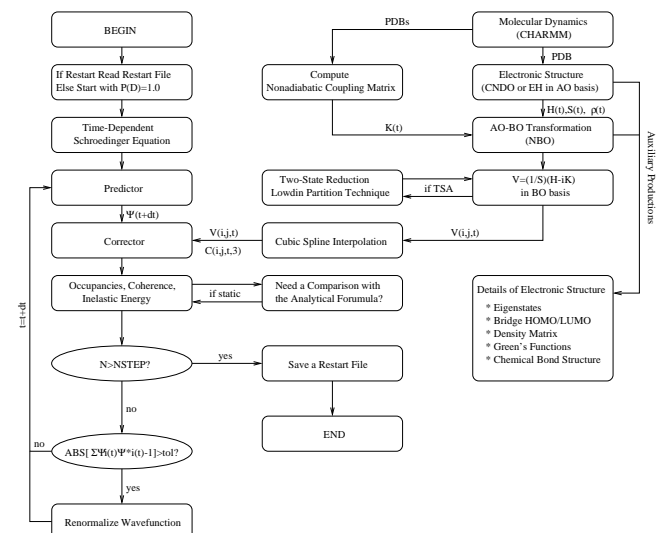
FIG. 7. The flowchart of the computer simulation. In this flowchart we assume that the integration of the Schrödinger equation is implemented by using a predictor-corrector method.

A. Molecular dynamics simulation for azurin

As has been pointed, we need to know the Hamiltonian, overlap and NAC matrices of the protein as a function

of time. We assume that the Hamiltonian at any time is simply the single-particle Hamiltonian derived from the protein conformation at that time. Prior to obtaining the above-mentioned matrices that guide the tunneling electron during the transfer process, a series of conformations were produced from an equilibrium MD trajectory. In this research, we employ the well established molecular simulation package CHARMM to perform the MD simulation for proteins.

The cystallographic structure of azurin[14] was taken from the Brookhaven Protein Database. The force field for the metalloprotein azurin, in addition to the general parameters provided by CHARMM for common animo acids, was taken from a paper by Voth and coworkers for another blue copper protein plastocyanin[15]. We modified some of the force field parameters to keep the bipyramidal geometry of the copper complex of azurin thermodynamically stable.

In order to get more natural dynamics, we performed solvent simulation for the whole azurin molecule, although we did not actually include any water molecule in our electronic structure calculations. Compared with a less time-consuming vacuum simulation, the existence of water simply makes the motion of the protein more confined and therefore the predicted atomic fluctuations will be smaller than those by a vacuum simulation.

To begin with, we prepared a cube of water, which contains $20 \times 20 \times 20$ unit cells. The length of the unix cell was chosen according to the density of water under room temperature and one atmospheric pressure. This cube of water was equilibrated at 300 K for 10000 AKMA time steps by standard Verlet algorithm using the periodic boundary conditions. All bonds and angles were shaken using the SHAKE command.

We put the azurin molecule, together with the crystallographic water molecules, in the center of the equilibrated water cube, and cut the cube into a sphere of a radius 28Å. A deformable stochastic boundary with a soft boundary potential and a stochastic buffer region[16] was introduced to contain the water molecules in the sphere. Any water molecule whose oxygen fell out of this sphere was deleted. Also those whose oxygen had a distance to the heavy atoms of the protein and crystallographic water shorter than 2.8Å were eliminated. All the water molecules (including the crystallographic water) were equilibrated with the protein being fixed for some time in order for them to redistribute energetically favorable around the protein.

The water sphere normally shrinked after some period of equilibration, the tips of the protein might therefore be exposed to vacuum. In order to avoid this, more water was added to keep the whole protein in well solvated condition. We did this in the following way: After a period of equilibration, the program paused for filling up the shrinkage and possible voids, the water cube (with a different SEGment name) was used to overlay the whole system, the new water molecules were concatenated with the old water by the JOIN command. After that we rotated the new system 90° and repeated the same overlaying procedure for two or three times. It was found that rotating the system brought more chances for filling, as expected the number of water molecules added to the solvent after each overlaying decreased when the times of rotation increased. The new water molecules were deposited in a new PDB file. We took the restarting coordinates from this new structure file and those for the protein and cystallographic water which were not changed, reassigned initial velocities for all the atoms, and equilibrated the new system. Checking the fluctuations of kinetic energy, potential energy, boundary potential and some geometries (e.g. bond lengths, bond angles, and dihedral angles), we found that the system had reached thermal equilibrium after 300 picoseconds of equilibration.
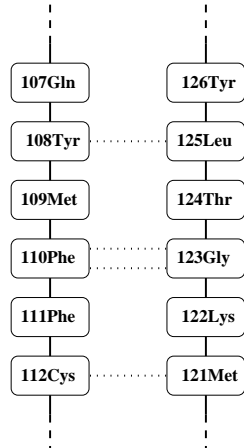
FIG. 8. Animo acid sequence of the β-sheet in azurin. The dotted lines between the two strands stand for the hydrogen bonds.

After equilibration, production trajectories started to be created, with a time steplength of one femtosecond. The whole protein is apparently too large for time-dependent electronic structure calculations. But in this paper we are interested in only the β-sheet portion formed by the Cys^{112}-Gln^{107} and Met^{121}-Thr^{126} β-strands (as is shown in Fig. 8), which has been the target of ET experiments. Therefore, we cut the β-sheet residues from the whole azurin and deposited them into a separate trajectory file while the simulation was being carried out. Instead of a simple hydrogen atom substitution, we applied the ACE and CT3 termini provided by CHARMM's topological input file to where a peptide bond was ruptured due to the truncation. Assume that we select a segment whose index runs from the n-th to the m-th residue, after the structure is pruned, the coordinates of C, CA and O in the $n-1$ residue are given to CY, CAY and OY in the ACE terminus, and those of N, CA and HN in the $m+1$ residue to NT, CAT and HNT in the CT3 terminus. The coordinates of the remaining six H atoms are determined by the HBUILD command (therefore the resultant geometries are somehow energet-

ically minimized). No significant rotation of the three H atoms around the axis perpendicular to the plane they form and through the carbon atom (CAY or CAT) was observed in both termini along the trajectory thus created. This is important for a time-dependent calculation, because a free rotating terminus, even being peripheral to the tunneling pathways, can constitute a large boundary perturbation, which may not be true in a real system.

B. Semiempircal electronic structure calculations

A large part of our simulation is to get the single-particle Hamiltonian matrices along a MD trajectory. In this research we employ both the extended-Hückel(EH) and complete neglect of differentail overlaps (CNDO) methods[17] to create the Hamiltonian matrices in the AO basis. The EH code was taken from QCPE 571:Extended Hückel Molecular, Crystal and Properties Package[18]; while the CNDO/S code was taken from QCPE 408: Bond Orbitals in the Neglect of Differential Overlap (BONDO) Approximation[19]. In the former method, the Hamiltonian is constructed directly from the overlap matrix elements: The diagonal elements are the ionization potentials of the atomic orbitals $H_{ii} = E_i$ and the off-diagonal elements are taken as $H_{ij} = (K/2)S_{ij}(E_i + E_j)$, where $K = 1.75$ is the Hückel constant. The latter method starts with a Hamiltonian which contains the primitive Hückel term and Coulombic contributions and requires a self-consistent field procedure. In our calculations, convergence is regarded achieved if the energy difference between two adjacent iterations is smaller than 5×10^{-5} hartree. In order to accelerate the iteration, computation of a conformation utilizes the converged density matrix of the last conformation, which was only one femtosecond before, as an input for constructing the initial Fock matrix (rather than constructing it from scratch). The current conformation normally does not differ drastically from the last one, since the protein structure changes little during a femtosecond. As a result, the number of iteration steps needed to reach self-consistence for each conformation can be reduced.

At present, we are unable to perform open-shell CNDO calculations. Therefore, we cannot treat proteins with metal ions as donor and acceptor at such a theoretical level. (Due to the same computational reason, residues with a positive charge is neutralized by removing a proton off.) So our donor and acceptor have to be chosen as two orbitals from the protein's electronic structure. And for mimicing photoexcited states, the orbital energies of these two orbitals have to be changed such that they fall into the energy gap of the protein. We found that if we did this in the AO basis, the bridge eigenstates would be significantly perturbed (since an AO has very strong couplings with other AOs, particularly those belonging to the same atom). Considering the usual assumption that the intercalation of donor and acceptor should not affect

the electronic structure of the bridge too much, an AO is not a well-defined donor or acceptor. Therefore, we employed the BO basis formed by using the NBO method. Changing local energetics in the BO basis hardly changes the bridge electronic structure. Additional advantages for using the BO basis are that sometimes we may need to distinguish electron and hole transfer and the BO basis provides an intuitive picture of chemical bonds which enables us to view ET in a way more consistent with the tunneling pathway model. In the following Subsection, we shall discuss the NBO method.

C. Transformation to the natural bond orbital basis

Having obtained the overlap, Hamiltonian and density matrices in the AO basis for an electronically saturated system, the next step is to transform everything from the AO to BO basis. Due to the localization nature of protein electronic structure, the major parts of the electronic wave functions of an atom seldom go far, rather they are always restricted to a range that contains a few neighboring atoms. (And thus chemical bonds are formed. Of course there are a few exceptions in which the electronic wave functions are delocalized, as we shall discuss later.) The localization character can be revealed if one diagonalizes the subblocks of the density matrix associated with a specific group of atoms, e.g., a pair of atoms. This thought was systematically developed into the NBO method. The idea of the NBO is to use those nearly fully occupied eigenstates of the subblocks in the density matrix involving relevant atoms to represent the lone pairs (LPs) of the atoms and the bicentral bonds between two atoms, and construct the corresponding antibonds for the known bonds, considering appropriate polarization.

A deficiency for the original BONDO program is that it is unable to handle animo acid residues that contain aromatic rings. The sub density matrix diagonalization scheme can find three fully occupied bonds if we diagonalize the subblock associated with the 24 AO's belonging to the six carbon atoms around the aromatic ring, after depleting all the known σ bonds, but the eigenvectors of these three eigenstates do not seem to form chemically reasonable bonds, and they are not numerically stable, i.e., they change somehow randomly from one conformation to another.

We describe here a method to construct the correct delocalized bonds for aromatic rings. Before constructing these delocalized orbitals, we find out all the possible LPs and bond pairs, deplete them from the density matrix, and pick up the indices of atoms which form an aromatic group. Then we take the three sp_2 hybrids of each carbon of each aromatic ring, and build the p_z orbitals from them according to the condition of orthonormality. All the hybrids including these newly built p_z's are symmetrically orthogonalized subsequently, and the bonding and antibonding orbitals other than the aromatic delo-

calized states are deposited in the transformation matrix (TM). The aromatic delocalized orbitals are formed using appropriate symmetry adapted linear combinations (SALCs) of the six $2p(\pi)$ valence orbitals and then deposited to the TM. In the TM, they are reordered to be prior to the LPs and right after the bond pairs and labeled as PB and PB*. This new TM is used to transform the density matrix and Hamiltonian from the AO to the BO basis. For all animo acids whose side chain has an aromatic ring, the diagonal elements of the corresponding subblocks of the BO density matrix are found very close to 2(fully occupied) for the three π^b, while those of the three π^* orbitals are very small. (For the benzene molecule which is highly symmetric, our method works perfectly: The occupancies of the three π^b are found almost 2 and those of π^* are found almost null.) This means that the delocalized bonds have been successfully formed. As expected, the antibond densities of low-lying π^* orbitals tend to be larger than those of others.

Fig. 9 shows a typical chemical bond energy profile (energies plotted against orbital indices) for two residues(ACE+Gly+CT3 and ACE+Phe+CT3) , calculated by using the CNDO method. The bond energies shown are the average values over two picoseconds, whereas the corresponding fluctuctions are shown in the lower panel. The bridge gap is calculated to be about 12 eV. It can be seen that: (1) The π and π^* bonds are energetically closer to the gap; (2) The same chemical group has approximately the same bond energies for its bonds which do not participate interactions with the exterior, e.g. the C=O double bonds and the two ACE (or CT3) termini, hence we can identify different sort of groups from the energy profile. Moreover, we would like to point out that the upper panel of Fig. 9 presents the static energy disorder of the protein's electronic structure, whereas the lower panel gives the information about the amplitude of the dynamic energy disorder, which sometimes refers to the time dependence of the energy profile[20]. Energy disorder is an important concept in the theory of electron transport in molecule wires[21].
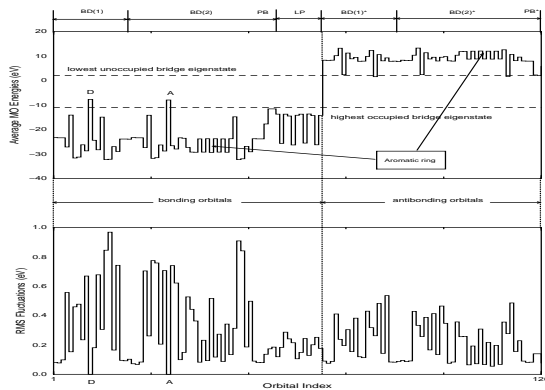
FIG. 9. Energy disorder profile of chemical bonds for two residues Gly[123] and Phe[110], obtained by the NBO method. The upper panel shows the average orbital energies(static energy disorder), the lower panel shows the corresponding root mean square fluctuations (dynamic energy disorder). The C_α-H_α bonds of the two residues are taken as the donor and acceptor. Their energies are lifted into the gap and kept resonant. "BD" stands for bond pairs, "BD*" for antibond pairs, "LP" for lone pairs, "PB" for aromatic π bonds, and "PB*" for aromatic π^* antibonds.

Fig. 9 shows that the bond energies are thermodynamically stable, but it does not describe the detailed bond structure. The full information about the chemical bonds defined by the NBO method is stored in the TM between the BO and AO bases. Let us assume the following vector represents a bond between two second row elements K and L: $(0, ., C_1^K, C_2^K, C_3^K, C_4^K, .., C_1^L, C_2^L, C_3^L, C_4^L, .., 0)$ (a row in the TM). All the irrelevant coefficients are zero except those corresponding to the two atoms, $C_i^{K,L}$ ($i = 1, 2, 3, 4$). The polarization factors for the two atoms are in fact $\rho_K = \sum_{i=1}^4 (C_i^K)^2$ and $\rho_L = \sum_{i=1}^4 (C_i^L)^2$, while the normalization condition requires that $\rho_K + \rho_L = 1$. We know that the molecular orbital has to be a linear combination of two somewhat distorted hybrid orbitals. In order to check if the hybrids are correct, the program renormalises for each individual atom the coefficents to one. For convenience we thereafter drop off the superscripts K and denote the renormalized coefficients as (C_1, C_2, C_3, C_4). The p-character and orientation angles for an atomic hybrid are defined as $P = 1/C_1^2 - 1$, $\Theta = \arctan(\sqrt{1 - \tilde{C}_4^2}/\tilde{C}_4)$, $\phi = \arctan(\tilde{C}_3/\tilde{C}_2)$, where $\tilde{C}_2, \tilde{C}_3, \tilde{C}_4$ are the renormalized coefficients (to a unit vector), i.e., $\tilde{C}_i = \tilde{C}_i/\sqrt{1 - C_1^2}$. We plot in Fig. 10 the fluctuations of polarization factors, p-characters and hybrid orientation angles of some typical bonds.

(a)

Fluctuation of a natural peptide bond C(110Phe)--N(111Phe)
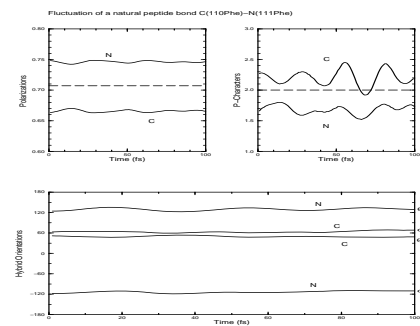
(b)
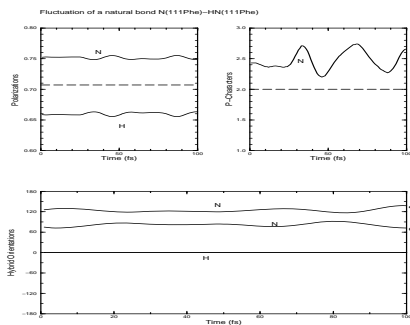
(c)
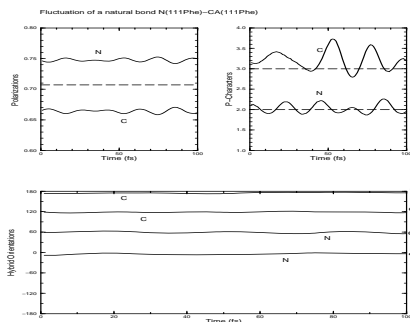
(d)
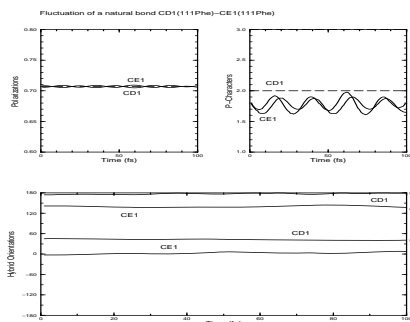
FIG. 10. Fluctuations of chemical bonds obtained by the NBO method. (a) The peptide bond between Phe[110] and Phe[111]; (b) N(Phe[111])-HN(Phe[111]); (c)N(Phe[111])-CA(Phe[111]); (d)A σ bond in aromatic ring: CD1(Phe[111])-CE1(Phe[111]).

Two major technical problems of the NBO method applied to a time-dependent study have to be emphasized here.

The first one is the bond orientation problem. As we know, the NBO method finds bonds by diagonalizations of individual subblocks. When it determines a bond, it does not "feel" the existence of the other subblocks. This does not result in a mistake for a single conformation computation, but in the time-dependent case it may lead to the following problem.

Imagine two bonds A and B which are associated with different subblocks but close enough to have a considerably big coupling, they are found by the NBO procedure as $|A\rangle = (0,.,A_1^K, A_2^K, A_3^K, A_4^K,.,A_1^L, A_2^L, A_3^L, A_4^L,.,0)$, $|B\rangle = (0,.,B_1^M, B_2^M, B_3^M, B_4^M,.,B_1^N, B_2^N, B_3^N, B_4^N,.,0)$, where it is implied that bond A is formed between two second-row atoms K and L, while bond B between M and N. Diagonalization of subblocks $K \otimes L$ and $M \otimes N$ gives two options which have opposite signs: $|A\rangle$, $-|A\rangle$ and $|B\rangle$, $-|B\rangle$. The diagonalization procedure chooses the one which satisfies a probably arbitrary criterion, say, the s component of the first atom must be positive, for a given conformation.

Now assume that one of the two bonds has small s characters (e.g. π bonds), $|A_1^K| \ll \max(|A_2^K|, |A_3^K|, |A_4^K|)$, $|A_1^L| \ll \max(|A_2^L|, |A_3^L|, |A_4^L|)$. Imagine for the next conformation at time $t + \delta t$, due to the local perturbation around K and L, the components evolve from $A_i^I(t)$ to $A_i^I(t + \delta t) = A_i^I(t) + \delta A_i^I (I = K, L; i = 1, 2, 3, 4)$. If the time step δ is small or the structural fluctuations are small, the increments are small $|\delta A_i^I| \ll 1$. Although they may not be able to change the signs of the big p components, they can change the signs of A_1^K and A_1^L since they are supposed to be small. Let us assume that $A_1^K(t) > 0$ while $A_1^K(t + \delta t) < 0$, it therefore has to be flipped, $A_1^K(t + \delta t) \to -A_1^K(t + \delta t)$, and as a result, the three p components of atom K and all components of atom L are flipped simultaneously, $A_i^K(t + \delta t) \to -A_i^K(t + \delta t)(i = 2, 3, 4); A_j^L(t + \delta t) \to -A_j^L(t + \delta t)(j = 1, 2, 3, 4)$. While this is not a big change for A_1^K and A_1^L, it is a big and perhaps unphysical change for the p components. On the other hand, let us assume that the local perturbation around M and N does not create an increment which is big enough to upset the sign of B_1^M. Everything continues smoothly for the B bond. Now, let us examine the coupling between the two bonds. At time t, it is $H_{AB}(t) = \langle A(t)|H(t)|B(t)\rangle$, at time $t + \delta t$, it becomes $H_{AB}(t + \delta t) = \langle A(t + \delta t)|H(t + \delta t)|B(t + \delta t)\rangle = \langle -A(t) + \delta A|H(t + \delta t)|B(t) + \delta B\rangle$. We see $H_{AB}(t + \delta t) \approx -H_{AB}(t)$, if the fluctuations are small. That is to say, the consequence of such a sign switching for eigenvectors is a sign switching for the corresponding couplings in the NBO Fock matrix. For aromatic rings, the SALCs will mispresent the delocalized state if the six p_z' orbitals do not point to the same direction. As a result, large occupanies in the antibonding orbitals will be observed.

The solution to this problem is to choose a reference conformation for which the NBO creates the bond structure correctly, save the orientations of all bonds into an information matrix, and impose these orientations to all bonds of all conformations involved in the calculation. For systems containing aromatic rings, one must make sure that there exists no phase difference among all the atomic hybrids of the six carbon atoms. This idea will presumably fail if there is a structural transformation or bond reformation, which is not very likely for a protein in thermal equillibrium.

11

The second problem is the degeneracy problem. The degeneracy problem arises when in a single subblock there are two bonds which are both fully populated. The diagonalization procedure may not be able to distinguish them: The eigenstates thus created may be mixed states. The C=O double bond and O LPs in each amino acid are such cases. Diagonalization of the sub density matrix of C=O cannot single out the σ, π bonds. Therefore, if we transform the Hamiltonian matrices of consecutive conformations along a MD trajectory to the BO basis, very large fluctuations of Hamiltonian matrix elements may be observed. This type of false fluctuations of Hamiltonian may influence the numerical stability of electronic dynamics.

Different from the problem of aromatic ring, which is a degeneracy problem too, the σ, π bonds cannot be built in a similiar way. Although we have known two sp_2 hybrids of C which take part in the formations of C-N and C-C_α bonds, the other sp_2 and the p_z orbitals cannot be constructed from the two known sp_2's by using only the condition of orthonormality. The method to repair this problem is to diagonalize the corresponding subblock of the Hamiltonian matrix, because σ, π bonds are not energetically degenerate. The eigenstates thus obtained would represent more correctly the bonds, and fluctuate less.

The same problem exists for the two LPs of oxygen of the CO group. Diagonalization of the one-center subblock belonging to the oxygen sometimes could not distinguish the two LPs very well. If we diagonalize the corresponding subblock of the Hamiltonian matrix, the following two states will be found $\phi_{LP1} = p'_y, \phi_{LP2} = 0.77s' + 0.64p'_x$, where the prime means the orbitals have been transformed to a local coordinate system. p'_y is perpendicular to the plane formed by the σ and π bonds of the C=O pair, which point in the local coordinate system to x' and z' respectively. If we further assume that the two LPs should be equivalent no matter how asymmetric the environment may be, we can build two equivalent LPs by simply taking linear combinations of ϕ_{LP1} and ϕ_{LP2}: $\psi_{LP1} = (1/\sqrt{2})(\phi_{LP1} + \phi_{LP2}), \psi_{LP2} = (1/\sqrt{2})(\phi_{LP1} - \phi_{LP2})$. The subblock in the transformed Hamiltonian matrix will have a nonzero off-diagonal element, which stands for the strong Coulombic repulsion between the two LPs.

When we transform from the AO basis the Schrödinger equation into the BO basis, the NAC matrices have to be transformed as well

$$K_{kl}^{BO}(t) = \sum_{ij} T_{ik}(t) \left[\dot{T}_{jl}(t) S_{ij}^{AO}(t) + T_{jl}(t) K_{ij}^{AO}(t) \right]$$

(22)

where $T_{ik}(t)$ is the TM element between the k-th BO and i-th AO states at time t, and $\dot{T}_{jl}(t)$ is the first-order time derivative of $T_{jl}(t)$.

D. The integrator

The time-dependent Schrödinger equation is integrated by using either the Gear predictor-corrector method or the classical Runge-Kutta method. The algorithms of the integrators require that $H(t)$, $S(t)$ and $K(t)$ be known at arbitary time t. It will be extremely time-consuming to calculate using quantum chemical approaches these matrices for each ET time step since δt_{ET} is usually of the magnitude 10^{-3} femtosecond in order not to diverge while the interested time scale for our computation is normally at the level of picoseconds (dependent on the Landau-Zener time). On the other hand, since the difference of the protein conformations may be small within a few δt_{ET} so that replacing the intermediate ones by interpolated ones may not result in a pronounced difference of electronic dynamics, it does not seem necessary to calculate the matrices every ET step. Rather we take a series of conformational snapshots from a MD trajectory every δt_{SP}, calculate only for these sample conformations the matrices H_n, S_n, K_n using quantum chemical methods while get $V(t)$ at arbitary time t using the cubic spline interpolation method.

Numerical error is an important issue about the integrator that is related to the long-range ET, which normally involves a system with hundreds or even thousands of orbitals and a very weak T_{DA}. Accumulating numerical error is inevitable for any integration method. The question though is, if the transfer probability within the Landau-Zener time goes smaller than the average error $|\langle \Psi(t)|\Psi(t)\rangle - 1|/N$, say 10^{-6}, due to a small T_{DA}, how can we distinguish it from numerical error? Indeed this question may point to a serious limit of any time-dependent ET simulation. That is when error propagation runs faster than electronic propogation to a very weak coupled state. In the case that there is no immediate answer to the question, we guess that less numerical error is allocated to states which gain smaller occupancies, namely, the distribution of occupancies is not affected too much by numerical error. Albeit we cannot prove it in a dynamic case, we can prove that this is basically true in a static case (while numerical error may have nothing to do with the time-dependence of Hamiltonian etc.), by comparing the result given by the integrator and that by the following analytical formula

$$P_{DA}(t) = \left| \sum_n \exp\left(-i\mathcal{E}_n t/\hbar\right) \langle A|\Psi_n\rangle \langle \Psi_n|D\rangle \right|^2 \quad (23)$$

where $\mathcal{E}_n$ is the eigenenergy of the n-th eigenstate, Ψ_n is the corresponding eigenvector. We found that when T_{DA} is of the magnitude of 10^{-5} eV, the results given by the two independent methods were almost the same (the latter method has much less numerical error and may be regarded as the strict result).

In this Section, we present the computer simulation results for ET dynamics in azurin. These results were obtained on the basis of two different levels of approximations (Tab. I). The first level possesses higher accuracy in electronic structure calculation, but it neglects differential overlaps and hence retarded(advanced) overlaps. In accordance with this, NACs are ignored in the subsequent electronic dynamics calculation. The second level is less precise in electronic structure calculation but it is on nonorthogonal basis and NACs are incorporated in electronic dynamics calculation.

With the framework of the second level, the effect of NACs on ET dynamics can be proven trivial as long as unphysical large fluctuations of basis set are inhibitted. This sort of false fluctuation does not exist in a time-dependent calculation in the AO basis. (In the AO basis, one can prove that a number of NACs turn out to be zero, see Appendix B.) As discussed carefully in Section V C, it originates from the NBO method with which we transform our simulation into the BO basis. As a matter of fact, one can estimate the upper bound for K_{ij} according to eq.(10). In a normalized basis, the maximum value for the right hand side of eq.(10) is $1/2\delta t$, so the magnitude of the NAC is $\hbar/(2\times\text{femtosecond})\approx 2$ eV. In reality, the difference of retarded and advanced overlaps is much less than 1, since a protein moves very little during a femtosecond (assuming that there is no ultrafast structural transition).

A major shortcoming of the EH method is that it severely underestimates the gap: The gap predicted by it is approximately 4 eV (ranging from -12 eV $\sim$ -8 eV), which disagrees with both higher level ab initio results and experimental results. By performing NBO analysis for the density matrix and Hamiltonian matrix given by the EH method, we found that the eigenstates falling into the interval between -12 eV and -2 eV are mainly contributed by the π^*s, and the populations residing at the π^*s are much bigger than those at the σ^*s (e.g. the populations for C=O antibonds are about 0.40, compared with normally less than 0.05 for σ^*s). Therefore, a simple trick to *remedy the EH method* is to reparametrize it in the BO basis, namely, to lift the orbital energies of π^*s out of the gap (We did this by adding 12 eV to the orbital energies of π^*s). The coupling matrix elements between the π^*s and others need not to change. Rediagonalizing the modified Hamiltonian matrix, we obtain a gap ranging from -12 eV to -2 eV, compared with -11 eV $\sim$ 1 eV predicted by the CNDO method.

TABLE I. Two levels of computer simulation.

Level	Orthonormality	Method	Nonadibatic Coupling
1	Orthonormal	CNDO/S	Ignored
2	Nonorthonormal	EH	Included

Since in this study we simply pick up two orbitals from the electronic structure of proteins as artificial donor and acceptor (in order to reduce the perturbation of such a choice to the side chains of the animo acids which are to accomodate our artificial donor and acceptor to the minimum, we select the C_α-H_α bonds as donor and acceptor; we hope this treatment would not jeopardize the general conclusions made in this research for dynamic ET reactions), the electronic structure of the bridge has to be explored in order to decide reasonable values for the energies of donor and acceptor and tunneling energy, which are normally inside the gap. Importantly, resonance of the energy level of donor and acceptor with any of the bridge eigenstates should be cautiously avoided (otherwise the electronic propogation will behave like transport in conductors rather than tunneling). For a fluctuating protein, care must be taken to prevent thermal motion from injecting electron into the bridge by crossing of either highest occupied molecular orbital (HOMO) or lowest unoccupied molecular orbital (LUMO) of the bridge with the energy levels of donor and acceptor. Fig. 11 shows typical thermal fluctuations of bridge HOMO and LUMO. The fluctuation amplitudes are around 0.4 eV. This implies that the energy level of donor and acceptor should be at least 0.2 eV above the average HOMO or below the average LUMO.
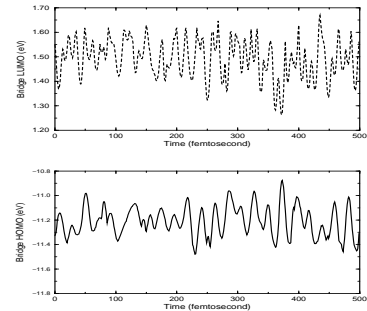
FIG. 11. Shown are the fluctuations of bridge HOMO and LUMO in a 500 *fs* MD segment, calculated by using the CNDO method. Donor was chosen as the C_α-H_α bond of Cys^{112} or Met^{121}. The C_α-H_α bonds of other residues were chosen as the acceptor. The bridge is the remainder of the electronic structure excluding the donor-acceptor orbital pair. The HOMO and LUMO of different bridges are indistinguishable in the figure.

It was also found that bridge HOMO and LUMO were not affected too much by the choice of donor and acceptor. In the calculations for Fig. 11, we have chosen the C_α-H_α bond of Cys^{112} or Met^{121} as the donor and selected other C_α-H_α bonds as the acceptors, the results of bridge HOMO and LUMO are virtually the same (to a few decimals). The invariance of bridge gap to the

choice of donor and acceptor comes from the following facts: First, in the BO basis, the Hamiltonian matrix is nearly diagonal; Second, the energies of C_α-H_α bonds are more or less close to each other. Eleminating such a pair of orbitals (out of a few hundreds) from such a system does not actually change the eigenenergies of the remaining states.
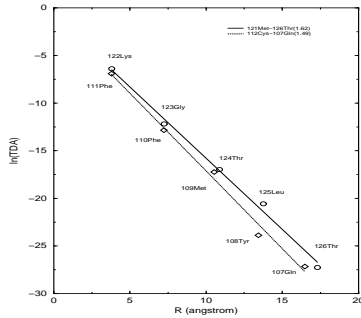
FIG. 12. T_{DA} exponentially decays along the β-sheet. For strand 107-112, donor: Cys^{112}; acceptors: Phe^{111}, Phe^{110}, Met^{109}, Tyr^{108} and Gln^{107}. For strand 121-126, donor: Met^{121}; acceptors: Lys^{122}, Gly^{123}, Thr^{124}, Leu^{125} and Thr^{126}. The tunneling energy was chosen as -10 eV. Calculated by the CNDO method, averaged over 0.5 picosecond.

The effective electronic coupling, T_{DA}, falls off rapidly with respect to the separation distance between donor and acceptor R_{DA}. The decay behavior is always described by an exponential function

$$T_{DA} \propto \exp\left(-\beta R_{DA}/2\right) \tag{24}$$

Experiments[3] revealed that for β-sheet the Cu^+ to Ru^{3+} distance-decay constant β is about 1.1 Å^{-1}. Our CNDO calculations show that for artificial donors and acceptors the average constant $\langle\beta\rangle \approx 1.5 \sim 1.6$ Å^{-1} if the tunneling energy is chosen as -10 eV. (Fig. 12).

B. Effect of bridge dynamics on electron transfer

To exclude the effect of donor and acceptor motion, we freeze the donor and acceptor energies and maintain them in the resonance regime. In such a way, the ET dynamics is purely assisted by the bridge motion and determined by its dynamical behavior. The effect of bridge dynamics can be investigated in the following way: (a) Select a segment of MD trajectory, find the resonace condition for donor and acceptor and calculate T_{DA} for the first conformation; (b) Put an electron on the donor site at time $t=0$, solve the time-dependent Schrödinger equation eq.(6) in accordance with the Hamiltonians etc. obtained for each conformation, get the transfer probability $P_{DA}(t)$; (c) Assume that from the starting point of the selected trajectory segment on, the system dynamics is suddenly frozen (imagine this procedure as something

like rapid quenching), in other words, the subsequent conformations are identical to the first one, repeat (b) (the transfer probability thus obtained is denoted by $P_{DA}^{qu}(t)$); (d) Do the TD2SA, namely, project the Hamiltonians etc. to a two-state form, and integrate the two-state quantum equation of motion eq.(17) (the transfer probability thus obtained is denoted by $P_{DA}^{2s}(t)$). It is expected that $P_{DA}^{qu}(t)$ will exhibit sinusoidal behavior since donor and acceptor have been tuned into resonance and there exists no force to push them off.
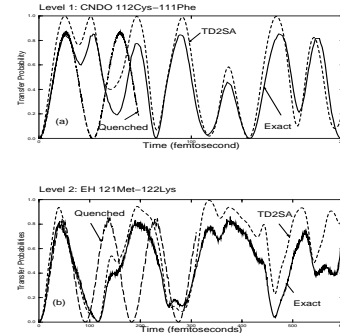
FIG. 13. Strong coupling cases ($\sqrt{\langle T_{DA}^2 \rangle} \sim 10^{-2}$ eV). (a) Level 1 calculation: Cys^{112}(D)-Phe^{111}(A). Donor and acceptor energies are about -10 eV (vicinal to the bridge HOMO), the tunneling energy is -9 eV. (b) Level 2 calculation: Met^{121}(D)-Lys^{122}(A). Donor and acceptor energies are about -11 eV (vicinal to the bridge HOMO), the tunneling energy is -10 eV. $P_{DA}(t)$, $P_{DA}^{2s}(t)$ and $P_{DA}^{qu}(t)$ are denoted by full lines, dashed lines and long dashed lines, respectively.
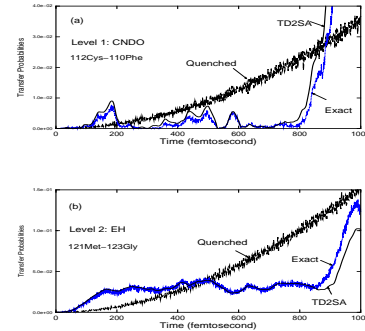
FIG. 14. $\sqrt{\langle T_{DA}^2 \rangle} \sim 10^{-3}$ eV. (a) Level 1 calculation: Cys^{112}-Phe^{110}. Donor and acceptor energies are about -10 eV, the tunneling energy is -9 eV. (b) Level 2 calculation: Met^{121}-Gly^{123}. Donor and acceptor energies are about -11 eV, the tunneling energy is -10 eV. $P_{DA}(t)$, $P_{DA}^{2s}(t)$ and $P_{DA}^{qu}(t)$ are denoted by dashed lines, full lines and long dashed lines, respectively.
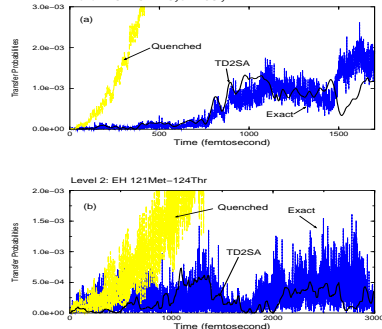
FIG. 15. $\sqrt{\langle T_{DA}^2 \rangle} \sim 10^{-4}$ eV. (a) Level 1 calculation: Cys^{112}-Gly^{123}. Donor and acceptor energies are about -10 eV, the tunneling energy is -9.5 eV. (b) Level 2 calculation: Met^{121}-Thr^{124}. Donor and acceptor energies are about -11 eV, the tunneling energy is -10 eV. $P_{DA}(t)$, $P_{DA}^{2s}(t)$ and $P_{DA}^{qu}(t)$ are denoted by dashed lines, full lines and long dashed lines, respectively.

Shown in Figs. 13, 14 and 15 are the ET probilities calculated by the exact method and the TD2SA method in the cases of different coupling strength at both computational levels. In Fig. 13, the donor and acceptor are so close that the direct interaction between them H_{DA} constitutes a large part of the total coupling $\mathcal{H}_{DA}$, which means that the through-space tunneling pathway is important. It can be seen from the figures that $P_{DA}(t)$ deviates from $P_{DA}^{qu}(t)$ after some time, whereas $P_{DA}^{2s}(t)$ roughly reproduces $P_{DA}(t)$ within a few hundred femtoseconds.

The significant difference between $P_{DA}(t)$ and $P_{DA}^{qu}(t)$ comes exactly from the effect of bridge dynamics on the ET dynamics, whereas the agreement between $P_{DA}(t)$ and $P_{DA}^{2s}(t)$ represents how well a ET dynamics can be approximated by a simple two-state picture. In fact, the two-state picture explains why $P_{DA}(t)$ differs from $P_{DA}^{qu}(t)$. In the two-state picture, donor and acceptor, now "dressed" with backscattering effect $T_{DD}(t)$ and $T_{AA}(t)$, fluctuate around the resonance energy levels (see the inset of Fig. 16). Such a two-state system certainly exhibits transfer behavior different from a sinusoidal one, which occurs when the system is resonant all along. We performed a series of similiar simulations on various MD trajectories and found that, for T_{DA} between 10^{-2} eV and 10^{-4} eV and within typical Landau-Zener time (up to a few picoseonds), there is no evidence that the bridge dynamics would always increase or decrease the transfer probability. For example, in Fig. 14, one can see sometimes $P_{DA}(t)$ is smaller than $P_{DA}^{qu}(t)$ but sometimes it is greater. This is somehow counterintuitive since it is readily surmised that a system remaining in resonance should have more chances to transfer than a system shuttling between on-resonance and off-resonance has. It hints that, the thermodynamics of an ET structure might be as important as its (static) energetics in determining its ET performance on specific conditions.
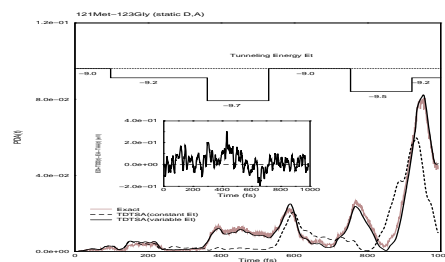
FIG. 16. The TD2SA can be improved by changing the tunneling energy from time to time (results of level 1 calculation). The dashed line is the result predicted by a TD2SA with a constant tunneling energy throughout the simulation, the solid line is that by a TD2SA with a variable tunneling energy, which almost reproduces the exact dynamics. The stair steps denote the change of tunneling energy. Shown in the inset is the fluctuation of the effective donor-acceptor energy difference, $\mathcal{H}_{DD}(t) - \mathcal{H}_{AA}(t)$, which is equivalent to the effect of multiple Landau-Zener crossing of some sort.

The TD2SA with a constant tunneling energy normally fails after a few hundred femtoseconds, but we found that by adjusting the tunneling energy E one would be able to improve the TD2SA if the system is not too coherent. Fig. 16 shows that by piecewisely tuning E, the TD2SA can reproduce unambiguously better the exact dynamical behavior. This leads to our conjecture that, the tunneling dynamics of a complicated system can always be described by the concise picture of TD2SA, provided that the time course of the tunneling energy is appropriately set. Hence the major task for a successful TD2SA may be the search of $E(t)$. At present, we find $E(t)$ by simply using the trial-error method. The result illustrated in Fig. 16 does not mean that $E(t)$ should necessarily follow a stepped route.

C. Dynamics of electron transfer between vibrating donor and acceptor

In the last Subsection we studied ET between frozen donor and acceptor and concluded that the TD2SA was valid. In this Subsection, we shall examine if the TD2SA is still valid in the case that donor and acceptor vibrate with natural frequencies. By the words "natural frequencies" we mean that the fluctuations of donor and acceptor energies are fully kept except that at the beginning of the simulation they are artificially "excited" into the gap. Like in the last Subsection, all the simulations begin with an initial condition that the donor site has an electron at time $t=0$.

In such cases, both the donor that initially carries the electron and the acceptor that is to receive the electron are moving. On one hand, since the system is in equilibrium, the donor and acceptor energies have many chances to cross (multiple Landau-Zener crossing). On the other hand, the resonance condition for donor and

acceptor does not make sense any more since it is only instantly satisfied in a vibrational period. In most time donor and acceptor are off-resonant. In the two-state picture, the fluctuations of the effective donor and acceptor energies are composed of those of $E_D(t), E_A(t)$ and $T_{DD}(t), T_{AA}(t)$. In the weakly-coupled limit, the relative energy level shift induced by the backscattering effect, $T_{DD}(t) - T_{AA}(t)$, is normally believed to be much smaller than that caused by orbital fluctuations, $E_D(t) - E_A(t)$. When the couplings turn stronger, the backscattering effect will turn out to be more important.

(a)

(b)
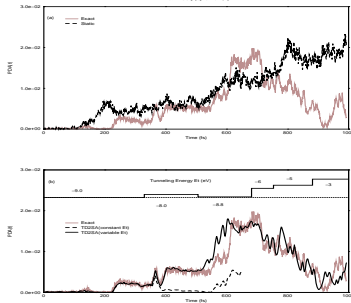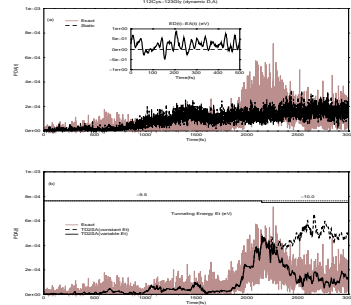
FIG. 17. Eletron transfer dynamics between vibrating donor and acceptor for $\sqrt{\langle T_{DA}^2 \rangle} \sim 10^{-3}$ and 10^{-4} eV, respectively (level 1 calculations). Shown in the upper panels of (a) and (b) are comparison of results in the absence of bridge motion and those in the presence of bridge motion (exact). Shown in the lower panels are comparison of the exact results with those by the TD2SA with a constant tunneling energy and variable tunneling energies. The inset in (b) shows typical temporal behavior of $E_D(t) - E_A(t)$.

Within the current framework, the effect of protein dynamics on ET consists of the effect from donor and acceptor motion and that from bridge motion. Freezing the bridge and carrying out simulation with only donor and acceptor moving can help us examine the latter effect. In the upper panels of Fig. 17 (a)(b) we show the comparisons of such results with the exact ones. The differences between them imply that even though the motion

of donor and acceptor themselves looks overwhelming, the delicate effect from bridge motion can be important in the time scale of up to a few picoseconds.

In the lower panel of Fig. 17 (a)(b), we show that the TD2SA with appropriately chosen time course of tunneling energy does well in reproducing the exact dynamics. Our experience based on a series of simulations suggests that it seems more difficult to find the right time course of tunneling energy that enables the TD2SA to reproduce the exact dynamics in the presence of donor and acceptor motion than in the absence of donor and acceptor motion (the case in Subsection VI B). We conjecture that the flexibility of donor and acceptor energies might result in the flexibility of the tunneling energy, which as a consequence increases the difficulty of finding the correct $E(t)$.

D. Three-center electron transfer dynamics

In Section IV we have shown that the ET dynamics of a static model three-center system can be reproduced by a 3SA. Here we would like to strengthen the effective three-state picture by showing that the validity of the 3SA in reproducing the exact ET dynamics holds in the time-dependent case.

We select three C_α-H_α bonds along the β-sheet as the three redox centers and calculate the transfer probabilities $P_{DM}(t)$(donor to intermediate state) and $P_{DA}(t)$(donor to acceptor). In all simulations for three-center systems, none of the three redox centers is frozen, everything else is left as produced by the CHARMM and electronic structure computations except that we deliberately put D, M and A at the same energy level into the gap for the initial conformation, like we have done for the two-center systems in Subsection VI C. To implement the TD3SA, we apply the three-center projection and solve eq. (21).

(a)
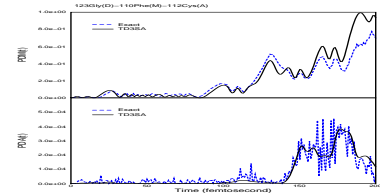
(b)
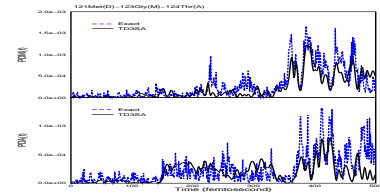
FIG. 18. Three-center ET dynamics in two systems (level 1). The dashed lines are exact results, whereas the full lines are TD3SA results. Tunneling energy is not changed throughout the period shown in the figures.

The simulations started with an initial condition on which the energies of the donor, the intermediate state, and the acceptor were all set to be -10 eV and an electron was introduced to the donor site. It is shown in Fig. 18 that for two three-center systems the TD3SA is basically able to describe the dynamical behavior of the systems for a certain length of time.

VII. CONCLUDING REMARKS

We have performed systematical computer simulations for ET dynamics in fluctuating protein. Based on the simulation results, we have found that it is not appropriate to ignore the effect of protein dynamics on electronic tunneling dynamics. We introduce an analogue of the well-known static two-state approximation, the time-dependent two-state approximation (and three-state approximation if three-center ET reaction is involved), and show that such a simple approximation is capable of reproducing the exact ET dynamics of the whole protein. Although we also have pointed out some issues which might be unaware before, for example, the importance of the backscattering matrix elements, it remains an open question how to incorporate these dynamic factors into the ET rate theory.

APPENDIX A

If $\mathcal{H}_{DD}$ and $\mathcal{H}_{AA}$ are off-resonant and the two-state Hamiltonian is time-independent, $\mathcal{H}_{DD}(t) = \mathcal{H}_{DD}$, $\mathcal{H}_{AA}(t) = \mathcal{H}_{AA}$, and $\mathcal{H}_{DA}(t) = \mathcal{H}_{DA}$, we have an analytical solution for the transfer probability

$$P_{DA}(t) = N_D(t_0)\frac{4\mathcal{H}_{DA}^2}{K^2}\sin^2\left(\frac{K(t-t_0)}{2\hbar}\right)$$

$$+N_A(t_0)\cos^2\left(\frac{K(t-t_0)}{2\hbar}\right) \tag{A1}$$

where $\delta = \mathcal{H}_{DD} - \mathcal{H}_{AA}, K = \sqrt{\delta^2 + 4\mathcal{H}_{DA}^2}$, $N_D(t_0)$ and $N_A(t_0)$ are the occupancies on the donor and acceptor

sites at time t_0, respectively. The two terms in the right hand side of eq.(A1) represent forward and back electron transfer. (Surprisingly the amplitude for the back electron transfer is independent on the driving force.) Eq.(A1) shows that in static case the backscatterings T_{DD} and T_{AA} may affect the maximum transfer probability, which equals $4\mathcal{H}_{DA}^2/[(\mathcal{H}_{DD} - \mathcal{H}_{AA})^2 + 4\mathcal{H}_{DA}^2]$. Since it is $\mathcal{H}_{DD} - \mathcal{H}_{AA} = H_{DD} - H_{AA} + T_{DD} - T_{AA}$ that actually determines $P_{DA}(t)$, $T_{DD} - T_{AA}$ may either reduce or enlarge the effective D-A energy difference and therefore enhance or weaken the ET rate. In the static case, only when $\delta = 0$ can a full tunneling occur. The smaller $\delta/\mathcal{H}_{DA}$ is, the greater the percentage of tunneling is. Since the Hamiltonian is static, the energy is conserved $\mathcal{E}(t) = \Psi_D^*(t)\Psi_D(t)\mathcal{H}_{DD} + \Psi_A^*(t)\Psi_A(t)\mathcal{H}_{AA} + [\Psi_D^*(t)\Psi_A(t) + \Psi_D(t)\Psi_A^*(t)]\mathcal{H}_{DA} = \mathcal{H}_{DD}$. From the energetic point of view, partial tunneling is easily understood: The conservation law of energy would be violated if an electron were fully transfered to the acceptor.

APPENDIX B

The NACs between two distinct $2p$ orbitals vanish: $K_{p_x p_y}(t) = K_{p_y p_z}(t) = K_{p_z p_x}(t) = 0$.
   Proof: Select p_x, p_z, rewrite $K_{p_x p_z}$ as

$$K_{p_x p_z}(t) = \sum_{\alpha=x,y,z} V_\alpha \langle p_x|\partial_\alpha p_z\rangle \tag{B1}$$

where V_α is the α component of the velocity of the atom.

$$\langle p_x|\partial_x p_z\rangle = \lim_{\delta\to 0}(1/2\delta)(\langle p_x(x,y,z)|p_z(x+\delta,y,z)\rangle$$

$$-\langle p_x(x,y,z)|p_z(x-\delta,y,z)\rangle)$$

$$\langle p_x|\partial_y p_z\rangle = \lim_{\delta\to 0}(1/2\delta)(\langle p_x(x,y,z)|p_z(x,y+\delta,z)\rangle$$

$$-\langle p_x(x,y,z)|p_z(x,y-\delta,z)\rangle)$$

$$\langle p_x|\partial_z p_z\rangle = \lim_{\delta\to 0}(1/2\delta)(\langle p_x(x,y,z)|p_z(x,y,z+\delta)\rangle$$

$$-\langle p_x(x,y,z)|p_z(x,y,z-\delta)\rangle)$$

$$\langle p_x(x,y,z)|p_z(x+\delta,y,z)\rangle = \langle p_{z'}(z',y',x')|p_{x'}(z'+\delta,y',x')\rangle$$

$$= \frac{3}{4\pi}\int_0^\infty (r')^2 dr' \int_0^\pi \sin\theta' d\theta' \int_0^{2\pi} d\phi'$$

$$\times R_{p_{z'}}(r')R_{p_{x'}}(\sqrt{(r')^2 + \delta^2 + 2r'\delta\cos\theta'})\cos\theta'$$

$$\times \frac{r' \sin\theta' \cos\phi'}{\sqrt{(r')^2 + \delta^2 + 2r'\delta\cos\theta'}} = 0$$

$$\langle p_x(x,y,z)|p_z(x,y+\delta,z)\rangle = \langle p_{x'}(x',z',y')|p_{y'}(x',z'+\delta,y')\rangle$$

$$= \frac{3}{4\pi} \int_0^\infty (r')^2 dr' \int_0^\pi \sin\theta' d\theta' \int_0^{2\pi} d\phi'$$

$$\times R_{p_{x'}}(r') R_{p_{y'}}\left(\sqrt{(r')^2 + \delta^2 + 2r'\delta\cos\theta'}\right) \sin\theta' \cos\phi'$$

$$\times \frac{r' \sin\theta' \sin\phi'}{\sqrt{(r')^2 + \delta^2 + 2r'\delta\cos\theta'}} = 0$$

$$\langle p_x(x,y,z)|p_z(x,y,z+\delta)\rangle = \frac{3}{4\pi} \int_0^\infty r^2 dr \int_0^\pi \sin\theta d\theta$$

$$\times \int_0^{2\pi} d\phi R_{p_x}(r) R_{p_z}\left(\sqrt{r^2 + \delta^2 + 2r\delta\cos\theta}\right) \sin\theta \cos\phi$$

$$\times \frac{r\cos\theta + \delta}{\sqrt{r^2 + \delta^2 + 2r\delta\cos\theta}} = 0$$

Therefore, $K_{p_x p_z}(t) = 0$. Q.E.D.

One can also see that the NACs between s and p orbitals are nonzero.

[1] S.S.Skourtis and D.N.Beratan, Adv. Chem. Phys. **106**, 377 (1999)

[2] D.N.Beratan, J.N. Betts, and J.N.Onuchic, Science **252**, 1285 (1991)

[3] R. Langen, I.-J. Chang, J.P. Germanas, J.H. Richards, J.R. Winkler, H.B. Gray, Science **268**, 1733 (1995)

[4] J.Wolfgang, S.M.Risser, S.Priyadarshy, and D.N.Beratan, J. Phys. Chem. **101**, 2986 (1997)

[5] I.Daizadeh, E.S.Medvedev, and A.A.Stuchebrukhov, Proc. Natl. Acad. Sci. USA **94**, 3703 (1997); E.S.Medvedev and A.A.Stuchebrukhov, J. Chem. Phys. **107**, 3821 (1997)

[6] Q. Xie, G. Archontis, and S. Skourtis, *Protein electron transfer: A numerical study of the effect of bridge motion on the transfer dynamics*, submitted to Chem. Phys. Lett. (1999)

[7] B.R. Brooks, R.E. Bruccoleri, B.D. Olafson, D.J. States, S. Swaminathan, and M. Karplus, J. Comp. Chem. **4**, 187(1983)

[8] J.P.Foster and F. Weinhold, J. Am. Chem. Soc., **102**, 7211(1980)

[9] M. Head-Gordon and J.C.Tully, J. Chem. Phys. **103**, 23 (1995)

[10] S. Hammes-Schiffer and J.C.Tully, J. Chem. Phys. **101**, 4657 (1995)

[11] S.S. Skourtis and S. Mukamel, Chem. Phys. **197**, 367 (1995)

[12] G. Iversen, Y. I. Kharkats, A. M. Kuznetsov, and J. Ulstrup, Adv. Chem. Phys. **106**, 453 (1999)

[13] A. K. Mazur, J. Phys. Chem. B **102**, 473 (1998)

[14] H. Nar, A. Messerschmidt, R. Huber, M. Van de Kamp, G.W. Canters, J. Mol. Biol. **218**, 427 (1991); Brookhaven Protein Data Bank entry "4AZU"

[15] L.W.Ungar, N.F.Scherer and G.A.Voth, Biophysics J. **72**, 5 (1997)

[16] C.L. Brooks III and M. Karplus, J. Chem. Phys. **79**, 6312 (1983)

[17] J.A.Pople, D.L.Beveridge, *Approximate Molecular Orbital Theory*, McGraw-Hill Book Co., New York, 1970

[18] M.-H. Whangbo, M.Evain, T.Hughbanks, M. Kertesz, S. Wijeyesekera, C. Wilker, C. Zheng, and R. Hoffman, *QCPE Program No. 571: Extended Hückel Molecular, Crystal and Properties Package* (Quantum Chemistry Program Exchange, Bloomington, Indiana).

[19] F. Weinhold, *QCPE Program No. 408: Bond Orbitals in the Neglect of Differential Overlap Approximation* (Quantum Chemistry Program Exchange, Bloomington, Indiana).

[20] L. D. A. Siebbeles and Y. A. Berlin, Chem. Phys. **238**, 97 (1998)

[21] M. Kemp, A. Roitberg, V. Mujica, T. Wanta, and M. A. Ratner, J. Phys. Chem. **100**, 8349 (1996)